AMERICAN SOCIETY FOR MICROBIOLOGY | Molecular and Cellular Biology®

RESEARCH ARTICLE

Impaired Skin Barrier Function Due to Reduced ω-*O*-Acylceramide Levels in a Mouse Model of Sjögren-Larsson Syndrome

Koki Nojiri,[a] Shuhei Fudetani,[a] Ayami Arai,[a] Takuya Kitamura,[a] Takayuki Sassa,[a] Akio Kihara[a]

[a]Laboratory of Biochemistry, Faculty of Pharmaceutical Sciences, Hokkaido University, Sapporo, Japan

Koki Nojiri, Shuhei Fudetani, and Ayami Arai contributed equally to this article. Author order was determined randomly.

ABSTRACT Sjögren-Larsson syndrome (SLS) is an inherited neurocutaneous disorder whose causative gene encodes the fatty aldehyde dehydrogenase ALDH3A2. To date, the detailed molecular mechanism of the skin pathology of SLS has remained largely unclear. We generated double-knockout (DKO) mice for *Aldh3a2* and its homolog *Aldh3b2* (a pseudogene in humans). These mice showed hyperkeratosis and reduced fatty aldehyde dehydrogenase activity and skin barrier function. The levels of ω-*O*-acylceramides (acylceramides), which are specialized ceramides essential for skin barrier function, in the epidermis of DKO mice were about 60% of those in wild-type mice. In the DKO mice, levels of acylceramide precursors (ω-hydroxy ceramides and triglycerides) were increased, suggesting that the final step of acylceramide production was inhibited. A decrease in acylceramide levels was also observed in human immortalized keratinocytes lacking *ALDH3A2*. Differentiated keratinocytes prepared from the DKO mice exhibited impaired long-chain base metabolism. Based on these results, we propose that the long-chain-base-derived fatty aldehydes that accumulate in DKO mice and SLS patients attack and inhibit the enzyme involved in the final step of acylceramide production. Our findings provide insight into the pathogenesis of the skin symptoms of SLS, i.e., decreased acylceramide production, and its molecular mechanism.

KEYWORDS aldehyde dehydrogenase, ceramide, ichthyosis, lipid, long-chain base, Sjögren-Larsson syndrome, skin, sphingolipid

Since aldehydes are highly electrophilic, they are reactive and thus toxic to cells and tissues in general. Therefore, aldehydes generated in living organisms must be promptly converted to other molecules with low reactivity, such as carboxylic acids. Aldehyde dehydrogenases (ALDHs) are enzymes that convert aldehydes to carboxylic acids. Humans and mice contain 19 and 21 ALDH isozymes, respectively (1, 2). There are several known inherited diseases caused by mutations in the *ALDH* genes (1, 3). One of these, Sjögren-Larsson syndrome (SLS; Mendelian Inheritance in Man [MIM] no. 270200), is caused by mutations in the gene encoding the fatty aldehyde dehydrogenase (FALDH) ALDH3A2, which is highly active toward fatty aldehydes (4, 5).

SLS is an autosomal recessive inherited neurocutaneous disorder whose major symptoms are ichthyosis in the skin and spastic paraplegia and mental retardation in the nervous system (6, 7). Ichthyosis is a type of keratosis, characterized by thickening, dryness, and desquamation of the skin. So far, over 100 different mutations in *ALDH3A2* have been reported in SLS patients, and the prevalence of SLS is estimated to be 0.4 in 100,000 (7, 8). Accumulated fatty aldehydes in SLS patients are thought to cause the SLS pathology (5). However, the detailed molecular mechanism of SLS pathogenesis, including which fatty aldehydes are involved and which enzymes are inhibited by the accumulated fatty aldehydes, is largely unknown.

Citation Nojiri K, Fudetani S, Arai A, Kitamura T, Sassa T, Kihara A. 2021. Impaired skin barrier function due to reduced ω-*O*-acylceramide levels in a mouse model of Sjögren-Larsson syndrome. Mol Cell Biol 41:e00352-21. https://doi.org/10.1128/MCB.00352-21.

Address correspondence to Akio Kihara, kihara@pharm.hokudai.ac.jp.

Received 18 July 2021
Accepted 2 August 2021
Accepted manuscript posted online 9 August 2021
Published 24 September 2021

We previously analyzed *Aldh3a2* knockout (KO) mice and found that they exhibited some behavioral abnormalities, including impaired motor function (9). This phenotype appeared to be related to the neurological symptoms of SLS. In the *Aldh3a2* KO brain, levels of the 2-hydroxy galactosylceramides important for myelin function and maintenance were reduced. However, these *Aldh3a2* KO mice did not show an SLS-like skin phenotype (10). FALDH activity was reduced to ~30% of the wild-type (WT) levels in the brains of *Aldh3a2* KO mice, but was similar to WT levels in the epidermis. *ALDH3A2* belongs to the *ALDH3* subfamily. Humans have three *ALDH3* subfamily members (*ALDH3A1*, *ALDH3A2*, and *ALDH3B1*), whereas mice have five. In addition to the three orthologs (*Aldh3a1*, *Aldh3a2*, and *Aldh3b1*), mice also express *Aldh3b2* (*ALDH3B2* is a pseudogene in humans) and the rodent-specific *Aldh3b3* (1, 2, 11). Of these ALDH3 subfamily members, only ALDH3A1/Aldh3a1 shows high activity toward medium-chain (C_5 to C_{10}) aldehydes; the others are highly active toward long-chain (C_{11} to C_{20}) aldehydes (11–13). Since *Aldh3b2* is the most abundantly expressed of the *Aldh3* subfamily members in the mouse epidermis (10), it may compensate for the loss of *Aldh3a2* in the *Aldh3a2* KO mouse epidermis, resulting in the absence of an SLS-like skin phenotype.

Skin has a permeability barrier function (skin barrier) that prevents the invasion of foreign substances such as pathogens and allergens into the body and the excessive evaporation of water from the body. Abnormalities in the skin barrier cause several skin disorders, such as increased vulnerability to infectious diseases, ichthyosis, and atopic dermatitis (14, 15). Skin is composed of the epidermis, dermis, and subcutaneous tissue, and the epidermis is further divided into the following four layers (in order from outermost to innermost): stratum corneum (SC), stratum granulosum (SG), stratum spinosum (SS), and stratum basale (SB) (16, 17). In the intercellular spaces of the SC, there is a multilayered lipid structure called the lipid lamellae, which plays a pivotal role in the formation of the skin barrier (16, 17). The major lipid components of the lipid lamellae are ceramides, cholesterol, and fatty acids (FAs) (17–19). Ceramides are the hydrophobic backbone of sphingolipids and are composed of a long-chain base (LCB) and an FA linked by an amide bond (19). The epidermis contains a variety of ceramide classes, among which the epidermis-specific ω-*O*-acylceramides (acylceramides) are essential for skin barrier function (17, 19). Acylceramides have a characteristic structure, namely, three hydrophobic chains consisting of linoleic acid attached to the ω-position of the FA portion of normal ceramides. All of the human genes involved in acylceramide synthesis cause ichthyosis when mutated (17, 19, 20). Furthermore, mice in which any of those genes have been knocked out exhibit neonatal lethality due to markedly impaired skin barrier function (17, 19, 21).

Aldh3a2 KO mice do not show a skin barrier defect under normal conditions (10), probably due to the functional overlap with *Aldh3b2*, and are therefore unsuitable as an SLS model for skin pathology. In the present study, we generated *Aldh3a2 Aldh3b2* double-knockout (DKO) mice as a faithful SLS model and analyzed the resulting skin phenotype. The DKO mice exhibited abnormalities in the skin barrier and decreased acylceramide levels. Furthermore, our results suggest that the transacylation reaction, the final step in the acylceramide synthesis pathway, was inhibited in these mice. These findings provide a novel insight into the molecular mechanism of SLS pathogenesis.

RESULTS

Reduced FALDH activity in the epidermis of *Aldh3a2 Aldh3b2* DKO mice. To generate *Aldh3a2 Aldh3b2* DKO mice to use as an SLS skin model, we first created *Aldh3b2* KO mice using the CRISPR/Cas9 system. We obtained *Aldh3b2* KO mice with an 8-bp deletion in exon 2 of *Aldh3b2* (Fig. 1A); these mice developed normally to adulthood. Next, *Aldh3b2* KO mice were crossed with previously generated *Aldh3a2*$^{+/-}$ mice (10) to obtain *Aldh3a2*$^{+/-}$ *Aldh3b2*$^{-/-}$ mice. Finally, DKO (*Aldh3a2*$^{-/-}$ *Aldh3b2*$^{-/-}$) mice were generated by crossing male and female *Aldh3a2*$^{+/-}$ *Aldh3b2*$^{-/-}$ mice. Since we observed no phenotypic differences between WT and *Aldh3b2* KO mice in any of the experiments we conducted, we used littermate *Aldh3b2* KO (*Aldh3a2*$^{+/+}$ *Aldh3b2*$^{-/-}$)

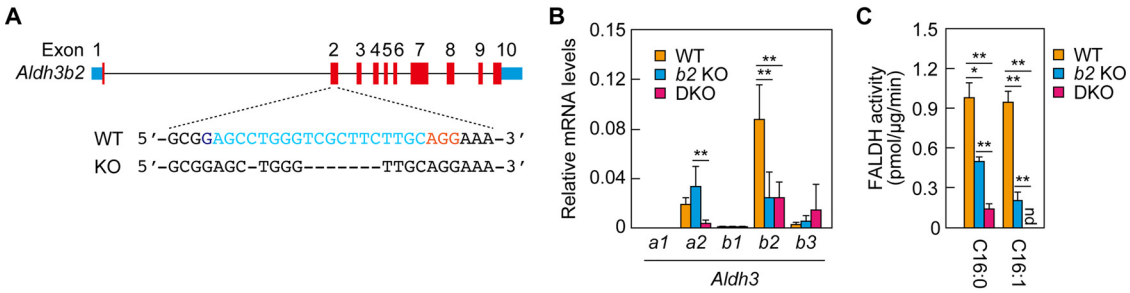

FIG 1 Creation of *Aldh3a2 Aldh3b2* double-knockout (DKO) mice and analysis of fatty aldehyde dehydrogenase (FALDH) activity. (A) *Aldh3b2* knockout (KO) mice were generated using the CRISPR/Cas9 system. The exon structure (red, coding sequence; blue, untranslated regions) of *Aldh3b2* and the nucleotide sequences of wild-type (WT) and *Aldh3b2* KO mice around the guide RNA target sequence (light blue) and the protospacer flanking motif (PAM) sequence (magenta) in exon 2 are shown. (B) Total RNA prepared from the epidermis of WT, *Aldh3b2* KO, and DKO mice was subjected to SYBR green-based quantitative real-time reverse transcription-PCR (RT-PCR) using specific primers for *Aldh3a1*, *Aldh3a2*, *Aldh3b1*, *Aldh3b2*, and *Aldh3b3*. Values are expressed relative to *Gapdh* and are the means ± standard deviation (SD) of three independent experiments. Statistically significant differences are indicated (**, $P < 0.01$; Tukey's test). (C) Total lysates (15 μg) prepared from the epidermis of WT, *Aldh3b2* KO, and DKO mice were incubated with 1.5 mM NAD^+ and 100 μM hexadecanal ($C_{16:0}$) or *trans*-2-hexadecenal ($C_{16:1}$) at 37°C for 30 min. The quantity of NADH product was determined by measuring the fluorescence of NADH (461.5 nm). Values presented are the means ± SD of three independent experiments. Statistically significant differences are indicated (*, $P < 0.05$; **, $P < 0.01$; Tukey's test). *b2* KO, *Aldh3b2* KO; nd, not detected.

mice as a control for the DKO mice in the following experiments. However, in some experiments, as an additional control, we present data from WT (C57BL/6J) mice born on the same day as the DKO mice.

Based on genotyping at 3 weeks of age, crosses between male and female *Aldh3a2*$^{+/-}$ *Aldh3b2*$^{-/-}$ mice generated 26 *Aldh3b2* KO mice (*Aldh3a2*$^{+/+}$ *Aldh3b2*$^{-/-}$) and 48 *Aldh3a2*$^{+/-}$ *Aldh3b2*$^{-/-}$ mice. No living *Aldh3a2 Aldh3b2* DKO (*Aldh3a2*$^{-/-}$ *Aldh3b2*$^{-/-}$) mice were observed. Genotyping during the brief postnatal period revealed that DKO mice were viable at birth and 1 day after birth but not beyond 2 days after birth. The numbers of *Aldh3b2* KO, *Aldh3a2*$^{+/-}$ *Aldh3b2*$^{-/-}$, and DKO mice on postnatal day 0 (P0) were 13, 35, and 16, respectively. All of the DKO mice had no milk in their stomachs and were left outside the nest, implying that they had been abandoned by their mothers.

To examine whether the expression of other *Aldh3* family members increased in a complementary manner in the *Aldh3b2* KO and DKO mice, we conducted real-time quantitative reverse transcription-PCR (RT-PCR) on the epidermis of P0 mice. In agreement with the results of our previous study (10), *Aldh3b2* was the most abundantly expressed *Aldh3* gene in WT mice, followed by *Aldh3a2* (Fig. 1B). In the *Aldh3b2* KO and DKO mice, expression levels of *Aldh3* family members other than the disrupted gene(s) were similar to those in WT mice, indicating no complementary increase in their expression. Expression levels of the disrupted genes were lower than those in WT mice (*Aldh3a2*, ~20% in DKO mice; *Aldh3b2*, ~30% in *Aldh3b2* KO and DKO mice), probably due to nonsense-mediated mRNA decay.

Next, we measured the FALDH activity toward $C_{16:0}$ (hexadecanal) and $C_{16:1}$ (*trans*-2-hexadecenal) aldehydes in the epidermis of WT, *Aldh3b2* KO, and DKO mice. In the *Aldh3b2* KO mice, activity toward $C_{16:0}$ and $C_{16:1}$ aldehydes was reduced to ~50% and ~20% of that in WT mice, respectively (Fig. 1C). In the DKO mice, activity toward $C_{16:0}$ aldehyde was reduced to ~15% of that in WT mice, and activity toward $C_{16:1}$ aldehyde disappeared completely. Considering our previous finding that FALDH activity in the epidermis of *Aldh3a2* KO mice was almost identical to that in WT mice (10), we conclude that Aldh3b2 and Aldh3a2 have overlapping FALDH activity, with Aldh3b2 being the predominant form in the mouse epidermis.

Decreased skin barrier function in DKO mice. At P0, the skin of the DKO mice looked rougher in texture than that of the *Aldh3b2* KO mice (Fig. 2A), and scanning electron microscopy revealed that their sulcus cutis was shallower than that of the *Aldh3b2* KO mice (Fig. 2B). We then investigated the neonatal lethality of DKO mice in

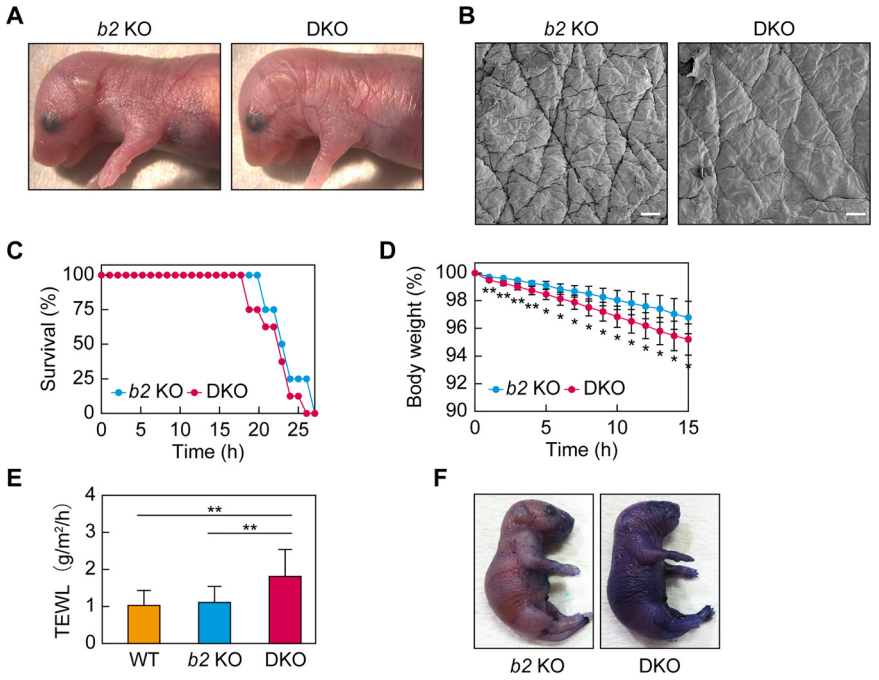

FIG 2 Impaired skin permeability barrier formation in *Aldh3a2 Aldh3b2* DKO mice. (A and B) *Aldh3b2* KO and DKO mice were photographed on postnatal day 0 (P0) (A) and subjected to scanning electron microscopy (B). Bars, 100 μm. (C and D) Time courses of survival rates (C) and body weights (D) of *Aldh3b2* KO (n = 4) and DKO (n = 8) mice after Caesarean section, examined at embryonic day 18.5 (E18.5). Values presented in panel D are means ± SD, and statistically significant differences from *Aldh3b2* KO mice are indicated (*, $P < 0.05$; **, $P < 0.01$; Student's t test). (E) Transepidermal water loss (TEWL) from WT (n = 8), *Aldh3b2* KO (n = 13), and DKO mice (n = 16) were measured at P0. Values presented are means ± SD, and statistically significant differences are indicated (**, $P < 0.01$; Tukey's test). (F) *Aldh3b2* KO and DKO mice at P0 were stained with 0.1% toluidine blue for 40 h and photographed. *b2* KO, *Aldh3b2* KO.

detail. DKO and *Aldh3b2* KO mice were prepared by Caesarean section at embryonic day 18.5 (E18.5), and their survival rate over time was measured. The control *Aldh3b2* KO mice died after 20 to 26 h (mean, 23.8 h) when they were kept away from their mother and unable to drink milk (Fig. 2C). This result was similar to our previous findings for WT mice (22, 23). The DKO mice died on average 1.5 h earlier than *Aldh3b2* KO mice, but this difference was not large enough to explain the neonatal lethality observed following natural birth. We also measured the time course of body weight. The DKO mice showed a slightly but significantly greater weight loss than that of *Aldh3b2* KO mice (Fig. 2D).

To determine whether this weight loss was due to greater water loss from the body, we measured transepidermal water loss (TEWL). We observed no difference between the WT and *Aldh3b2* KO mice, but the DKO mice exhibited approximately double the TEWL of these lines, suggesting reduced inside-to-outside skin barrier function (Fig. 2E). Next, we investigated the outside-to-inside skin barrier function using toluidine blue staining. Under long-term (40-h) staining, darker staining was observed in the DKO mice than that in the *Aldh3b2* KO mice (Fig. 2F). These results indicate that the DKO mice exhibited weak skin barrier abnormalities.

Hyperkeratosis in DKO mice. To investigate the cause of the skin barrier abnormalities in DKO mice, we performed a histological analysis of the epidermis via hematoxylin and eosin staining. In the epidermis of the control *Aldh3b2* KO mice, we observed gaps in the SC (Fig. 3A). These gaps represent the areas where lipid lamellae were originally present and are generated by the lipid elution that occurs during the alcohol dehydration step of the staining procedure. It has been reported that such gaps are

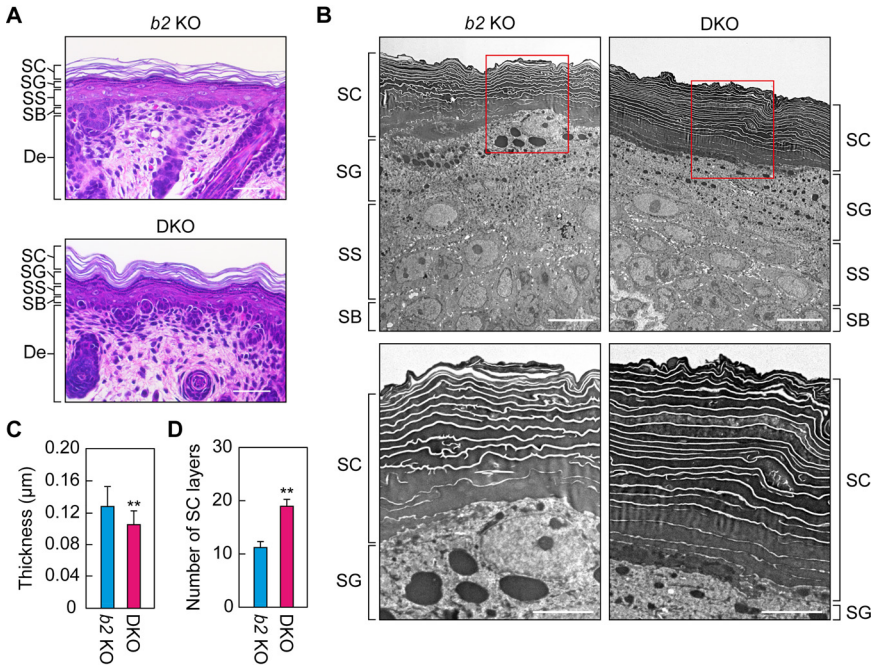

FIG 3 Hyperkeratosis and narrowed lipid lamellae in the *Aldh3a2 Aldh3b2* DKO mouse epidermis. (A) Paraffin sections (4 μm) of skin prepared from *Aldh3b2* KO and DKO mice at P0 were subjected to hematoxylin and eosin staining, and bright-field images were obtained. Bars, 50 μm. (B to D) Ultrathin sections (80 nm) of skin prepared from *Aldh3b2* KO and DKO mice at P0 were subjected to transmission electron microscopy. The lower images are enlarged views of the red rectangles in the upper images. Bars, 10 μm (upper panels) or 5 μm (lower panels). Lipid lamella thickness (C) and number of stratum corneum (SC) layers (D) were quantified from five different images. Values presented are means $\pm$ SD, and statistically significant differences are indicated (**, $P < 0.01$; Student's *t* test). SG, stratum granulosum; SS, stratum spinosum; SB, stratum basale; *b2* KO, *Aldh3b2* KO.

absent in mice with defective lipid lamella formation (22–24). In the epidermis of the DKO mice, we did observe gaps in the SC, although they appeared to be slightly narrower than those in the *Aldh3b2* KO mice (Fig. 3A).

We used transmission electron microscopy analysis to obtain more detailed views of the epidermis. Similar to the results described above (Fig. 3A), the lipid lamellae were slightly but significantly narrower in the DKO epidermis than in the *Aldh3b2* KO epidermis (Fig. 3B and C). Furthermore, the number of cell layers in the SC of the DKO mice was approximately twice that in the *Aldh3b2* KO mice (Fig. 3D). Such hyperkeratosis in the SC and abnormalities in the formation of the lipid lamellae have also been observed in SLS patients (25). The DKO mice therefore exhibited an SLS-like skin phenotype and are thus useful as a model for SLS skin pathology.

Decrease in acylceramide levels in the epidermis of DKO mice. Since the formation of the lipid lamellae was impaired in the DKO mice, we analyzed the lipid composition of the epidermis. Lipids were prepared from WT, *Aldh3b2* KO, and DKO mice at P0 and were separated via thin-layer chromatography (TLC), followed by detection using copper phosphate reagent. There were no obvious differences in lipid composition between the WT and *Aldh3b2* KO mice (Fig. 4A). However, in the epidermis of the DKO mice, we observed lower quantities of acylceramides and (*O*-acyl)-ω-hydroxy FAs (OAHFAs), which may be degradation products of acylceramides, and higher quantities of ω-hydroxy (ω-OH) ceramides, which are precursors of acylceramides. The quantities of other lipids were similar to those in the WT and *Aldh3b2* KO mice.

We next performed detailed quantitative analyses of the lipids, especially those that differed between mouse lines in the above TLC analyses, using liquid chromatography-tandem mass spectrometry (LC-MS/MS). Although total acylceramide levels were almost

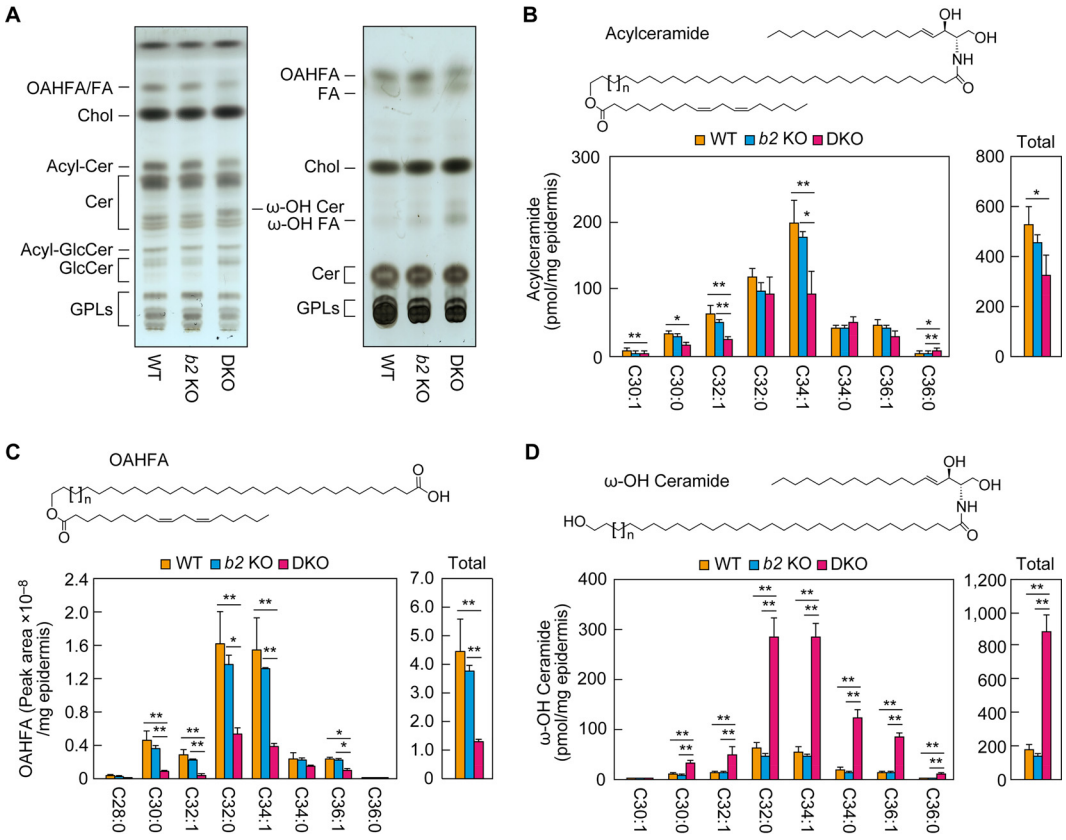

FIG 4 Reduced acylceramide levels in the *Aldh3a2 Aldh3b2* DKO mouse epidermis. (A) Lipids extracted from the epidermis of WT, *Aldh3b2* KO, and DKO mice at P0 were separated via thin-layer chromatography (TLC) using two different solvent systems suitable for the separation of ceramides (left) and less polar lipids (right). Lipids were stained with copper phosphate reagent. Acyl-Cer, acylceramide; Acyl-GlcCer, acyl-glucosylceramide; Cer, ceramide; Chol, cholesterol; GlcCer, glucosylceramide; GPL, glycerophospholipid. (B to D) Lipids were extracted from the epidermis of WT (n = 3), *Aldh3b2* KO (n = 3), and DKO (n = 3) mice at P0, and acylceramides (B), OAHFAs (C), and ω-OH ceramides (D) were analyzed via liquid chromatography-tandem mass spectrometry (LC-MS/MS). The quantities of each lipid species (according to chain length and saturation) and of total lipids are shown in the left and right panels, respectively. Values presented are means ± SD (*, $P < 0.05$, **, $P < 0.01$; Tukey's test). The structure of each type of lipid is shown above the graph. *b2* KO, *Aldh3b2* KO.

identical in the WT and *Aldh3b2* KO mice, those in the DKO mice were lower (~60% those of WT mice) (Fig. 4B), consistent with the TLC results (Fig. 4A). Acylceramides include multiple species that differ in the chain length and degree of saturation of the ω-OH FA moiety. The quantities of $C_{32:1}$ and $C_{34:1}$ acylceramides in particular were greatly reduced, to approximately half of WT levels (Fig. 4B).

The quantities of many molecular species of linoleic acid-containing OAHFAs—the putative degradation products of acylceramides—were also lower in the epidermis of the DKO mice than in the WT and *Aldh3b2* KO mice, with the total being approximately ~25% of that in the WT mice (Fig. 4C). In contrast, the quantities of almost all molecular species of ω-OH ceramides—the precursors of acylceramides—were greater in the epidermis of the DKO mice than in those of the WT and *Aldh3b2* KO mice, and the total quantity of ω-OH ceramides was approximately five times that in the WT mice (Fig. 4D). In the final step of acylceramide production, acylceramides are produced from ω-OH ceramides by a transacylation reaction (26). Our results—increased precursors (ω-OH ceramides) and decreased products (acylceramides)—suggest that this transacylation reaction is inhibited in DKO mice. Acylceramides are essential for skin barrier function, and all of the genes involved in their synthesis can cause ichthyosis when mutated (17, 19, 21). Therefore, it is highly likely that the abnormalities we observed in

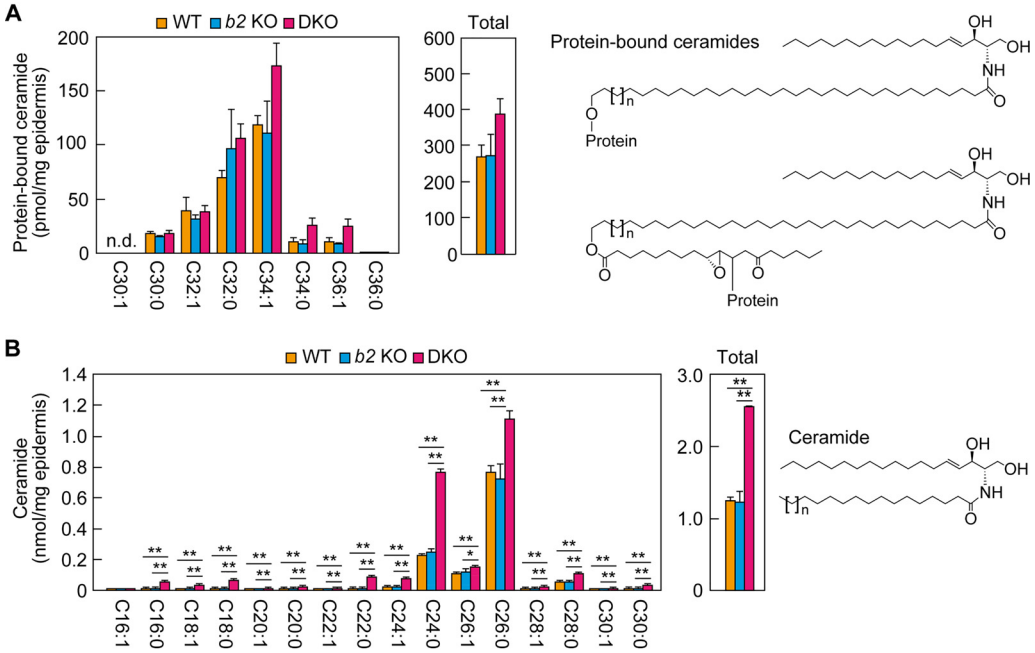

FIG 5 Levels of protein-bound and nonacylated ceramides in the *Aldh3a2 Aldh3b2* DKO mouse epidermis. (A and B) Lipids were extracted from the epidermis of WT ($n = 3$), *Aldh3b2* KO ($n = 3$), and DKO ($n = 3$) mice at P0, and protein-bound ceramides (A) and ceramides (B) were analyzed via LC-MS/MS. The quantities of each lipid species (according to chain length and saturation) and of total lipids are shown in the left and right panels, respectively. Values presented are means ± SD (*, $P < 0.05$; **, $P < 0.01$; Tukey's test). The structure of each type of lipid is shown to the right of the graph. The structure of a conventional protein-bound ceramide and that of a newly proposed one (28) are shown (upper and lower structures in panel A, respectively). *b2* KO, *Aldh3b2* KO; n.d., not detected.

skin barrier formation in the DKO mice were caused by these reduced acylceramide levels.

Normal levels of protein-bound ceramides in DKO mouse epidermis. Some of the acylceramides are converted to protein-bound ceramides, which bind covalently to the surface proteins of corneocytes (fully differentiated keratinocytes) (27, 28). Protein-bound ceramides are a component of a cell surface structure, the corneocyte lipid envelope (CLE), and are important for the formation of the skin barrier (29). We next quantified protein-bound ceramides using LC-MS/MS. Although acylceramide levels were reduced in the epidermis of the DKO mice (Fig. 4B), there were no significant differences in the quantities of protein-bound ceramides among the WT, *Aldh3b2* KO, and DKO mice (Fig. 5A). This result is consistent with the ultrastructure of the epidermis of SLS patients, in which the CLE structure is normal (25). Therefore, the reduced skin barrier function in DKO mice can be attributed only to the reduced acylceramide levels.

Next, we quantified normal (nonacylated) ceramides using LC-MS/MS. Again, we found no difference in quantities or composition between the WT and *Aldh3b2* KO mice, but in the DKO mice, the quantities of almost all molecular species were higher than those in the other two lines, and the total ceramide quantity was approximately doubled (Fig. 5B). This is likely to be a compensatory response to the reduced acylceramide levels.

Higher triglyceride levels in the epidermis of DKO mice. In the final step of acylceramide production, linoleic acid is transferred from triglycerides (TGs) to ω-OH ceramides via transacylation (26). In the DKO mouse epidermis, levels of ω-OH ceramides (one of the substrates of the transacylation reaction) were higher than those in the other two mouse lines (Fig. 4D). We next examined the quantities of linoleic acid-containing TGs (another substrate of the transacylation reaction) using LC-MS/MS. The WT and the *Aldh3b2* KO mice exhibited similar quantities and compositions of TGs (Fig. 6A). However, in the epidermis of the DKO mice, the quantities of many TG species

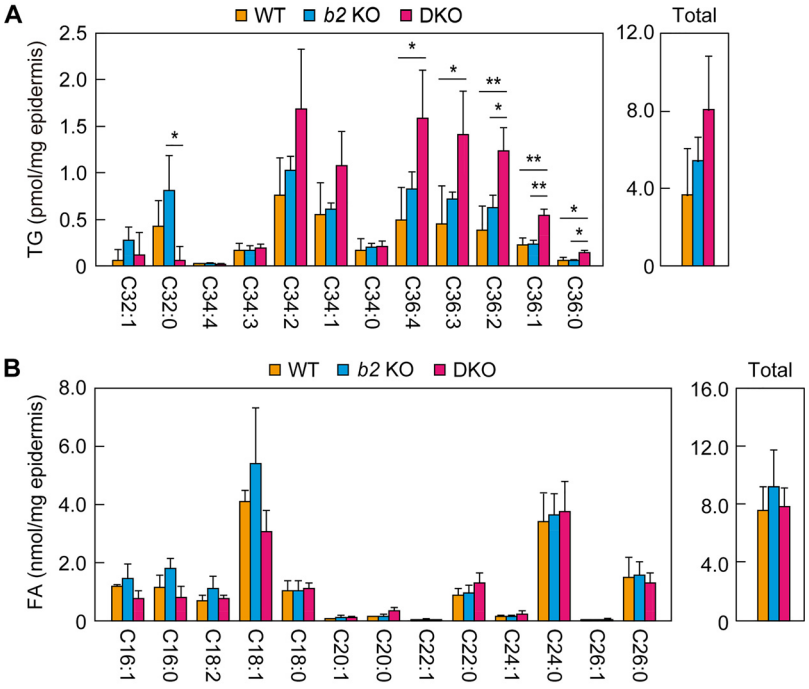

FIG 6 Levels of triglycerides (TGs) and fatty acids (FAs) in the *Aldh3a2 Aldh3b2* DKO mouse epidermis. (A and B) Lipids were extracted from the epidermis of WT ($n = 3$), *Aldh3b2* KO ($n = 3$), and DKO ($n = 3$) mice at P0, and linoleic acid ($C_{18:2}$)-containing TGs (A) and FAs (B) were analyzed via LC-MS/MS. The quantities of each lipid species (according to chain length and saturation) and total lipids are shown in the left and right panels, respectively. The chain lengths in panel A represent the sum of the two FAs other than linoleic acid. Values presented are means ± SD (*, $P < 0.05$; **, $P < 0.01$; Tukey's test). *b2* KO, *Aldh3b2* KO.

were greater than those in the WT and *Aldh3b2* KO mice. The total quantity of linoleic acid-containing TGs in the DKO mice was about double that in the WT mice, although this difference was not statistically significant. We also quantified free FAs in the epidermis, but there were no differences in their quantities, including that of linoleic acid, among the WT, *Aldh3b2* KO, and DKO mice (Fig. 6B). These results indicate that the reduced acylceramide levels in the epidermis of the DKO mice were not caused by a decrease in the levels of the substrates (ω-OH ceramides or TGs).

Decreased acylceramide levels in the SC of DKO mice. In the above-described analyses, we measured lipids prepared from the whole epidermis. Next, we focused on the lipids in the SC, which plays the most important role in skin barrier formation in the epidermis. The SC was isolated from the backs of *Aldh3b2* KO and DKO mice at P0 by tape stripping, and the lipids were extracted and subjected to LC-MS/MS to measure the acylceramides, ω-OH ceramides, ceramides, and protein-bound ceramides. As in the epidermis, acylceramide levels in the SC of the DKO mice were ~60% of those of the *Aldh3b2* KO mice (Fig. 7A). The quantities of both ω-OH ceramides and ceramides were again higher in the DKO mice (Fig. 7B and C), but at 2.6- and 1.6-fold, respectively, these differences were less pronounced in the SC than in the epidermis. The quantities of protein-bound ceramides were similar in the *Aldh3b2* KO and DKO mice (Fig. 7D). The results obtained for the epidermis and the SC were thus similar with respect to ceramide composition.

Normal expression levels of acylceramide synthesis-related genes in the DKO mouse epidermis. The final reaction in the acylceramide synthesis pathway is transacylation, which transfers the linoleic acid in TGs to ω-OH ceramides. The decrease in acylceramides and the increase in the substrates (ω-OH ceramides and TGs) in the epidermis/SC of DKO mice suggest that the activity of the enzyme(s) catalyzing this transacylation reaction was reduced. This reaction is catalyzed by the transacylase PNPLA1

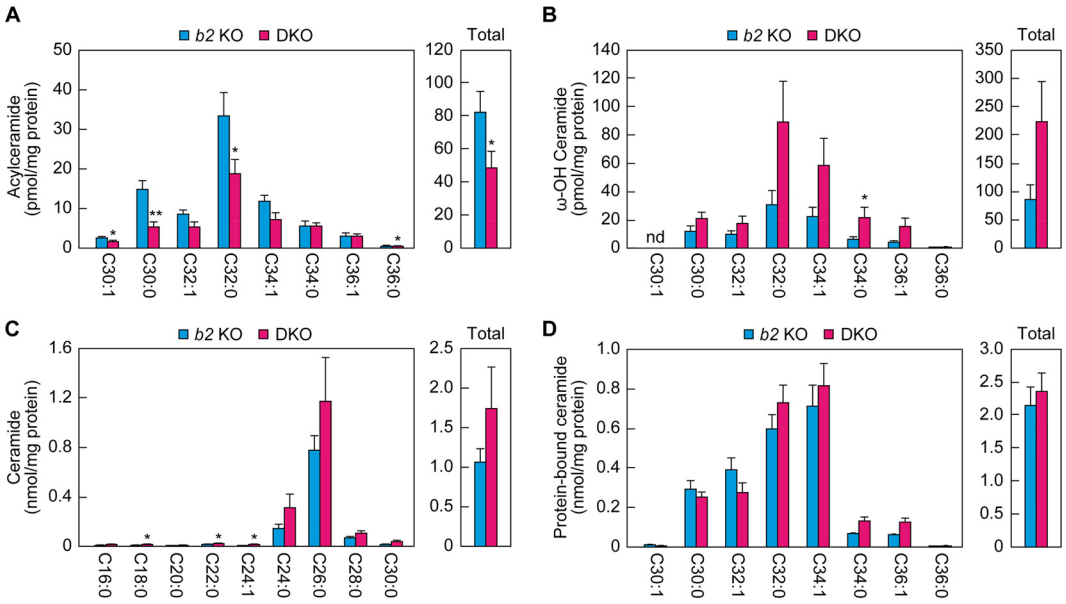

FIG 7 Reduced acylceramide levels in the SC of *Aldh3a2 Aldh3b2* DKO mice. (A to D) The SC was prepared via tape stripping from *Aldh3b2* KO ($n = 3$) and DKO ($n = 3$) mice at P0. Lipids were extracted, and acylceramides (A), ω-OH ceramides (B), ceramides (C), and protein-bound ceramides (D) were analyzed via LC-MS/MS. The quantities of each lipid species (according to chain length and saturation) and of total lipids are shown in the left and right panels, respectively. Values presented are means ± SD (*, $P < 0.05$; **, $P < 0.01$; Student's *t* test). *b2* KO, *Aldh3b2* KO; nd, not detected.

(26), and the α/β hydrolase family protein ABHD5 enhances the PNPLA1-catalyzed reaction, probably by stimulating the utilization of TG by PNPLA1 (30). There are two possible causes for this postulated decrease in enzyme activity, namely, a reduced quantity of enzyme(s) or inhibition of the enzyme(s). We investigated the former possibility—that the lower production of acylceramides in the DKO mouse epidermis was due to the lower expression levels of *Pnpla1* or *Abhd5* mRNA. Real-time quantitative RT-PCR revealed that both *Pnpla1* and *Abhd5* mRNA levels were comparable in the WT, *Aldh3b2* KO, and DKO mice (Fig. 8A). Similarly, the expression levels of other genes involved in acylceramide synthesis (those encoding FA ω-hydroxylase [*Cyp4f39*], acyl-CoA synthetase [*Fatp4*], and ceramide synthase [*Cers3*]), as well as those of keratinocyte differentiation markers (the basal layer marker keratin 5 [*Krt5*] and the spinous layer/granular layer markers keratin 1 [*Krt1*], loricrin [*Lor*], and involucrin [*Ivl*]), were similar in the three mouse lines (Fig. 8A and B). These results indicate that the reduced acylceramide levels in the DKO mouse epidermis were not the result of lower expression levels of genes involved in acylceramide synthesis.

Altered LCB metabolism in differentiated keratinocytes from DKO mice. One of the major species of fatty aldehydes in keratinocytes is long-chain aldehydes derived from LCBs, such as *trans*-2-hexadecenal, derived from sphingosine, and hexadecanal, derived from dihydrosphingosine (DHS) (10). LCBs produced during the *de novo* sphingolipid synthesis pathway or the degradation pathway of sphingolipids/ceramides are metabolized to complex sphingolipids (such as sphingomyelin or glycosphingolipids) or glycerolipids (ester-linked types) (Fig. 9A) (19, 31). In the LCB-to-glycerolipid metabolic pathway, LCBs are converted to LCB 1-phosphates, then to long-chain aldehydes by sphingosine 1-phosphate lyase, and further to long-chain FAs by FALDH. We have previously shown that the conversion of long-chain aldehydes to long-chain FAs in *Aldh3a2*-deficient CHO-K1 cells, neurons, and undifferentiated keratinocytes is impaired (9, 10, 31). In these cells, long-chain aldehydes are instead metabolized to long-chain alcohols, followed by conversion to ether-linked glycerolipids (such as plasmanyl/plasmenyl ethanolamine).

We performed a [^{3}H]DHS labeling assay to investigate LCB metabolism in keratinocytes

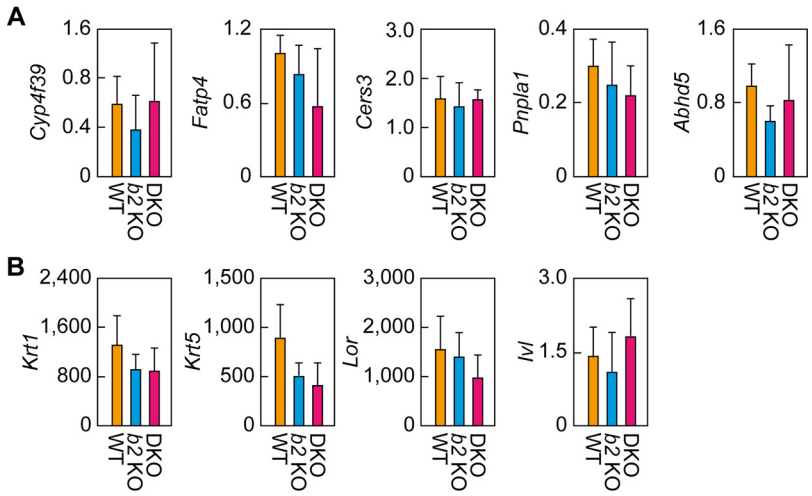

FIG 8 Expression levels of acylceramide synthesis-related genes and keratinocyte differentiation markers. (A and B) Total RNA prepared from the epidermis of WT (n = 3), *Aldh3b2* KO (n = 3), and *Aldh3a2 Aldh3b2* DKO (n = 3) mice at P0 was subjected to SYBR green-based quantitative real-time RT-PCR using specific primers for acylceramide synthesis-related genes (*Cyp4f39*, *Fatp4*, *Cers3*, *Pnpla1*, and *Abhd5*) (A) and keratinocyte differentiation markers (*Krt1*, *Krt5*, *Lor*, and *Ivl*) (B). Values are expressed relative to *Hprt1* and are means ± SD. *b2* KO, *Aldh3b2* KO.

prepared from the DKO mice. In undifferentiated keratinocytes from WT mice, DHS was metabolized to sphingolipids (ceramide, glucosylceramide, and sphingomyelin) and ester-linked glycerolipids (phosphatidylethanolamine, phosphatidylserine, phosphatidylinositol, phosphatidylcholine, and TG) (Fig. 9B). As previously reported (10), in undifferentiated keratinocytes from *Aldh3a2* KO mice, the metabolism of DHS to ester-linked glycerolipids was reduced, and instead ether-linked glycerolipids (plasmanyl/plasmenyl ethanolamine and 1-alkyl/alkenyl-2-acyl-glycerol) were produced. Through alkaline treatment, which hydrolyzes ester bonds, FAs were released from the ester-linked glycerolipids, whereas 1-alkyl/alkenyl-glycerol and its phosphoethanolamine adduct were released from the ether-linked glycerolipids. The metabolism of DHS was normal in undifferentiated keratinocytes from the *Aldh3b2* KO mice. However, undifferentiated keratinocytes prepared from the DKO mice also exhibited the abnormal metabolism of DHS to ether-linked glycerolipids that was observed in *Aldh3a2* KO keratinocytes, but at greater levels than those in the KO keratinocytes.

We then performed the [^{3}H]DHS labeling assay on differentiated keratinocytes. The DHS metabolism in these cells prepared from the *Aldh3a2* KO and *Aldh3b2* KO mice was similar to that in WT mice (Fig. 9C), but in cells from the DKO mice, we observed metabolism of DHS to ether-linked glycerolipids. Thus, the keratinocytes from the DKO mice exhibited impaired LCB metabolism regardless of whether they were differentiated or not, implying that abnormalities in LCB metabolism are responsible for the pathogenesis of skin symptoms in SLS.

Acylceramide levels in human keratinocytes reduced by *ALDH3A2* KO. To investigate whether FALDH deficiency also causes a decrease in acylceramide levels in humans, we disrupted *ALDH3A2* in human immortalized keratinocytes using CRISPR/Cas9. We obtained two *ALDH3A2* KO clones (KO 1 and KO 2) (Fig. 10A). These KO keratinocytes and two controls (controls 1 and 2) were differentiated, and the levels of acylceramides and ceramides were measured via LC-MS/MS. The quantities of acylceramides of all chain lengths were greatly reduced in both types of KO keratinocyte compared to those in the control keratinocytes (Fig. 10B). The total quantities in the KO keratinocytes were approximately 10% of those in the controls. With regard to the ceramides, the quantities of some species (as identified by chain length) were higher in the KO keratinocytes than in the controls, and those of others were lower, but the total quantities were similar (Fig. 10C). These

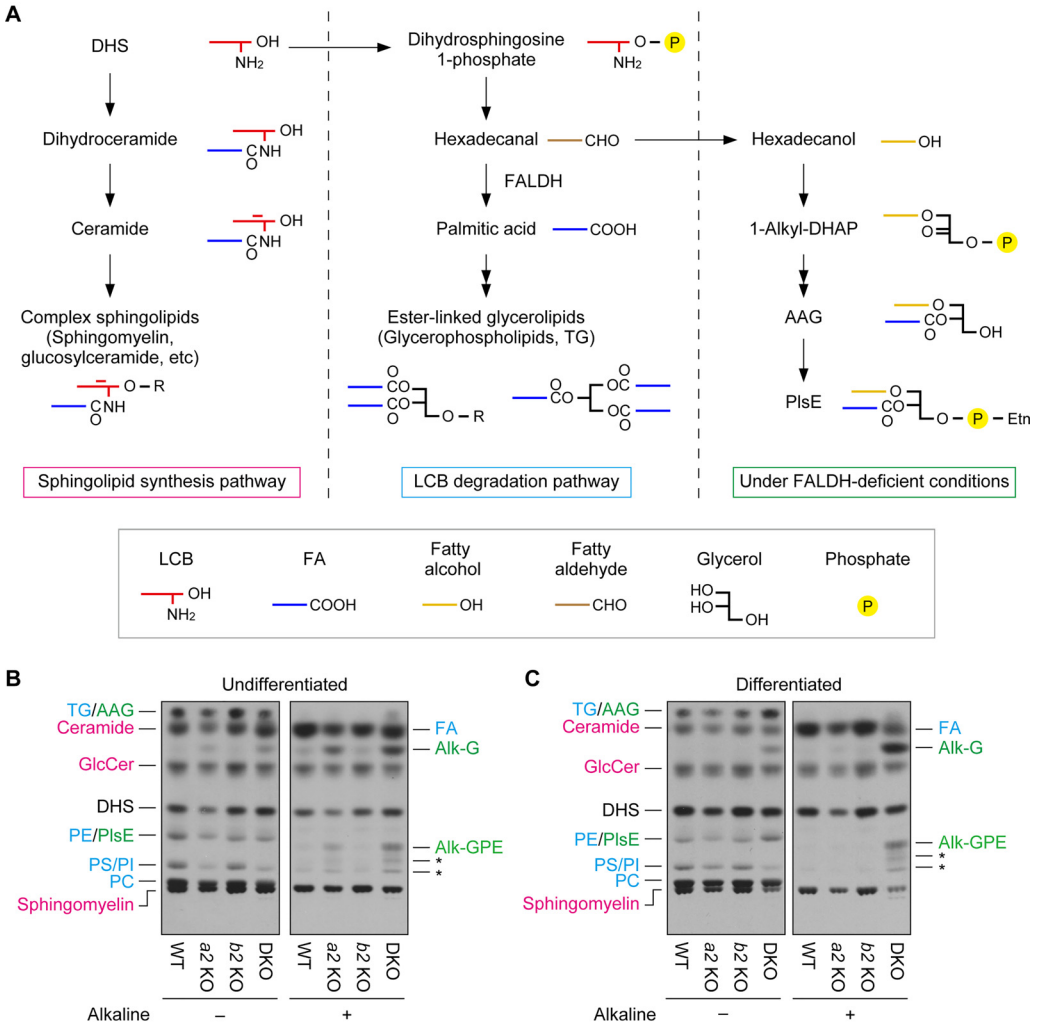

FIG 9 Impaired long-chain base (LCB) metabolism in *Aldh3a2 Aldh3b2* DKO mouse keratinocytes. (A) Metabolism of dihydrosphingosine (DHS) is illustrated. Under normal conditions, DHS is metabolized to complex sphingolipids in the sphingolipid synthesis pathway (left) or to ester-linked glycerolipids in the degradation pathway (middle). However, under FALDH-deficient conditions, such as *ALDH3A2* mutation in humans and *Aldh3a2 Aldh3b2* DKO in mice (right), the conversion of DHS to ester-linked glycerolipids is impaired, and DHS is instead metabolized to ether-linked glycerolipids. The simplified structure of each lipid is also shown. AAG, 1-alkyl/alkenyl-2-acyl-glycerol; DHAP, dihydroxyacetone phosphate; PlsE, plasmanyl/plasmenyl phosphatidylethanolamine; R, polar head group. (B and C) Primary keratinocytes were prepared from WT, *Aldh3a2* KO, *Aldh3b2* KO, and DKO mice, and undifferentiated (B) and differentiated (C) keratinocytes were labeled with [^{3}H]DHS at 37°C for 4 h. Lipids were extracted, given alkaline treatment or left untreated, separated via TLC, and detected using autoradiography. Asterisks indicate unidentified products of PlsE resulting from alkaline treatment. The colors represent lipids generated via the sphingolipid synthesis pathway (magenta) or the LCB degradation pathway under normal conditions (blue) or FALDH-deficient conditions (green). Alk-G, 1-alkyl/alkenyl-glycerol; Alk-GPE, 1-alkyl/alkenyl-glycerophosphoethanolamine; GlcCer, glucosylceramide; PC, phosphatidylcholine; PE, phosphatidylethanolamine; PI, phosphatidylinositol; PS, phosphatidylserine; *a2* KO, *Aldh3a2* KO; *b2* KO, *Aldh3b2* KO.

results indicate that FALDH deficiency causes a decrease in acylceramide levels in both mice and humans.

DISCUSSION

ALDH3A2 is the causative gene of SLS, and *Aldh3a2* KO mice have been analyzed previously as a model of SLS (9, 10). In the brain, FALDH activity toward $C_{16:0}$ aldehyde in *Aldh3a2* KO mice is reduced to ~30% of that in WT mice, and *Aldh3a2* KO mice exhibit neuronal phenotypes, such as motor dysfunction (9). However, in the epidermis, FALDH activity is not reduced in *Aldh3a2* KO mice, due to functional overlap with

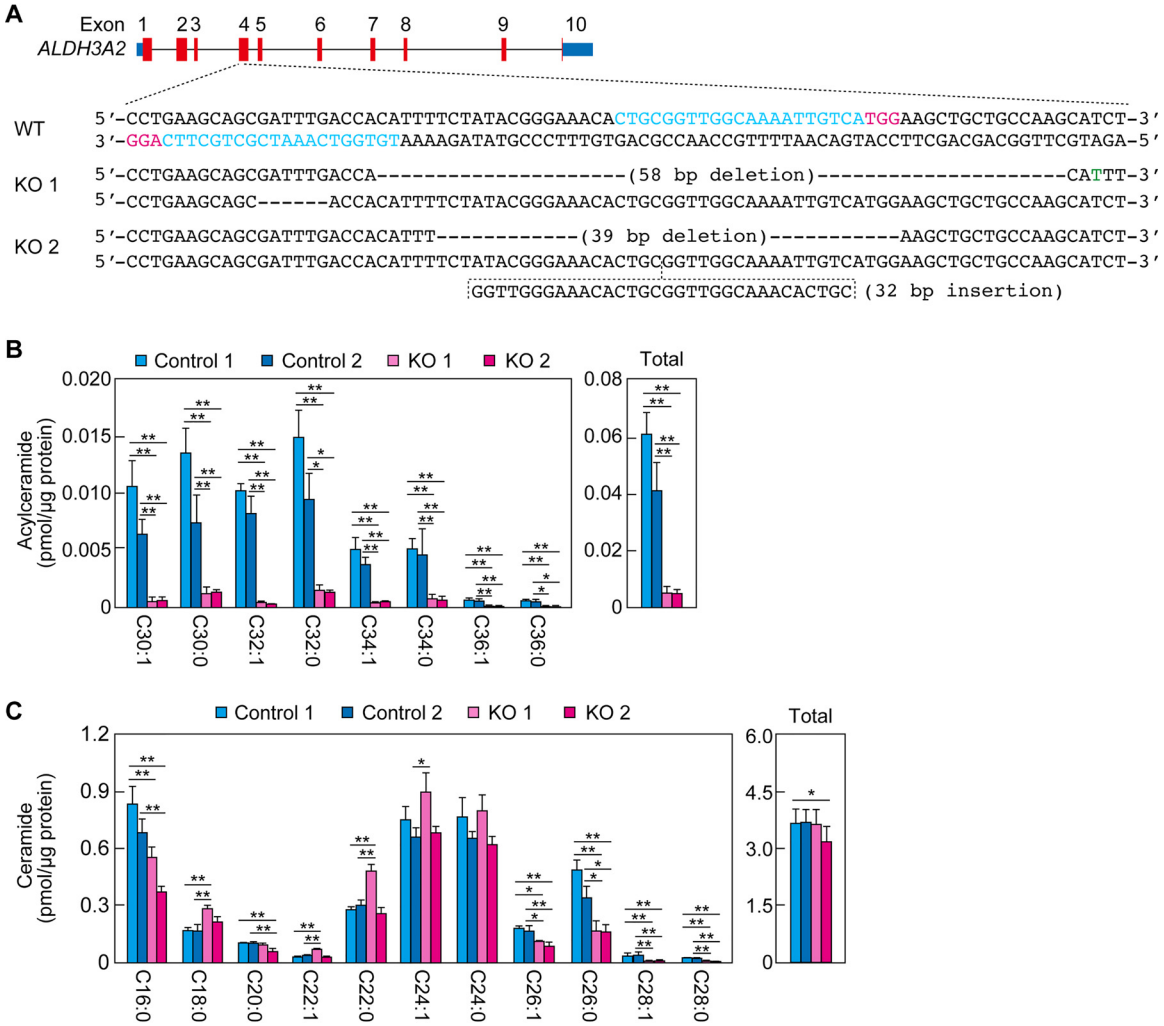

FIG 10 Reduced acylceramide levels in *ALDH3A2* KO human immortalized keratinocytes. (A) *ALDH3A2* KO keratinocytes were generated using the CRISPR/Cas9 system. The exon structure (red, coding sequence; blue, untranslated regions) of human *ALDH3A2* and the nucleotide sequences of WT and *ALDH3A2* KO cells (KO clones 1 and 2) around the guide RNA target sequences (light blue) and the PAM sequences (magenta) in exon 4 are shown. The green nucleotide indicates a missense mutation. (B and C) Lipids were extracted from two control cells and two *ALDH3A2* KO cells on day 14 of differentiation, and acylceramides (B) and ceramides (C) were analyzed via LC-MS/MS. The quantities of each lipid species (according to chain length and saturation) and of total lipids are shown in the left and right panels, respectively. Values presented are means ± SD (*, $P < 0.05$; **, $P < 0.01$; Tukey's test) from three independent experiments.

Aldh3b2, and the skin barrier function under nonstressed conditions is normal (10). In the present study, we generated *Aldh3a2 Aldh3b2* DKO mice and found that they exhibited phenotypes similar to the skin symptoms observed in SLS patients (decreased skin barrier function and hyperkeratosis) (Fig. 2 and 3), confirming that these mice are useful as a faithful SLS pathological model.

The abundance of acylceramides in the epidermis and SC of these DKO mice was ~60% of that in WT mice (Fig. 4 and 7). Reduced acylceramide levels have also been reported in SLS patients (32) and observed in *ALDH3A2* KO human keratinocytes (Fig. 10). Analyses of KO mice for the genes involved in acylceramide synthesis or other ichthyosis-causing genes have shown that there is a good correlation between the degree of reduction in acylceramide levels and the degree of skin barrier abnormality (22, 24, 33). In the epidermis of our DKO mice, in line with the partial reduction of acylceramide levels (~60% of those of WT mice) (Fig. 4 and 7), the degree of abnormality in the skin barrier function was mild (Fig. 2). In the epidermis of the DKO mice, the only lipids that

were reduced were acylceramides and their putative degradation products, OAHFAs (Fig. 4 to 7). We therefore speculate that this reduced abundance of acylceramides is the primary cause of the impaired skin barrier function seen in these DKO mice.

None of the DKO mice survived beyond 2 days after birth under natural delivery conditions. They had no milk in their stomachs, and many of them were abandoned outside the nest. Among the mice born by Caesarean section, the DKO mice died 1.5 h earlier, on average, than the control mice (Fig. 2C). However, this slight difference was not sufficient to explain the neonatal lethality of the naturally born DKO mice. Therefore, it is likely that this neonatal lethality is not caused by water loss from the body due to the abnormal skin barrier formation but is mainly due to abandonment by the mother. The appearance (different skin morphology) or odor of the DKO mice may lead to this behavior by the mother. Such abandonment of their babies by mother mice has also been reported in ceramide synthase *CerS3* KO mice (34), and it appears to be common in mice with defective acylceramide production.

The pathology of SLS is thought to be caused by the toxicity of accumulated fatty aldehydes, especially long-chain aldehydes, which are the substrates of ALDH3A2 (11, 12). Aldehydes generally form Schiff bases with primary amines, such as those in Lys and Arg residues. Furthermore, α,β-unsaturated aldehydes are more toxic than normal aldehydes, since the double bond that is conjugated with the carbonyl group can react with amino acid residues that have general nucleophiles, such as His, Cys, or Trp residues, via a Michael addition reaction (35, 36). In the brain and epidermis of SLS patients, certain proteins with important functions in these tissues are thought to be attacked by the accumulated long-chain aldehydes, resulting in the inhibition of their activities. What proteins are actually inhibited in SLS patients? Since ALDH3A2 is an endoplasmic reticulum (ER) protein (37), *ALDH3A2* mutations may cause the accumulation of long-chain aldehydes in the ER membrane. Therefore, it is highly likely that the target proteins of the aldehydes are ER membrane proteins. Among these, candidates are proteins that allow long-chain aldehydes to enter the active site, i.e., enzymes whose substrates are long-chain lipids, and those that have nucleophilic active-site residues that can be attacked by aldehydes. We previously found fatty acid 2-hydroxylase (FA2H) to be such a candidate target in the nervous system, via analyses of *Aldh3a2* KO mice (9). FA2H is an ER membrane protein and has His residues in its active site (38, 39). It catalyzes the production of 2-OH FAs using long-chain FAs as the substrates (40). 2-OH FAs are precursors of 2-OH galactosylceramides, which play an important role in myelin (41, 42).

In the epidermis of the DKO mice, acylceramide levels were reduced, but levels of the substrates ω-OH ceramides and TGs were enhanced (Fig. 4 and 6). These results suggest that the transacylation reaction that produces acylceramides from ω-OH ceramides and TGs was inhibited in these mice (Fig. 11). This reaction is catalyzed by the transacylase PNPLA1, and the α/β hydrolase family protein ABHD5 seems to enhance TG utilization of PNPLA1 (26, 30). It is likely that ABHD5 also promotes TG utilization of the TG lipases ATGL/PNPLA2 and PNPLA3 (43, 44). *PNPLA1* and *ABHD5* are the causative genes of autosomal recessive congenital ichthyosis and the syndromic form of ichthyosis Dorfman-Chanarin syndrome, respectively (17, 20, 45, 46). Since the expression levels of *PNPLA1* and *ABHD5* were unchanged in the epidermis of the DKO mice (Fig. 8A), it is likely that the activity of one of the proteins they encode, not the quantity, was reduced. Analyses of KO mice for these genes revealed that TG levels are normal in the *Pnpla1* KO mouse epidermis, whereas they are increased in the *Abhd5* KO mouse epidermis (47). Considering that the levels of many TG species were increased in our DKO mice (Fig. 6A), we speculate that ABHD5 is inhibited by the accumulated long-chain aldehydes due to impaired FALDH activity. ABHD5 belongs to the α/β hydrolase family, and members of this family generally have three catalytic residues: a nucleophile (Ser, Cys, or Asp), an acidic amino acid (Asp or Glu), and His (45). However, in ABHD5, the nucleophilic residue is replaced by Asn, resulting in no hydrolytic activity. Instead, ABHD5 may retain the ability to bind TGs and present them to the PNPLA proteins. ABHD5 is localized at the interface between lipid droplets and the ER (30) and has a

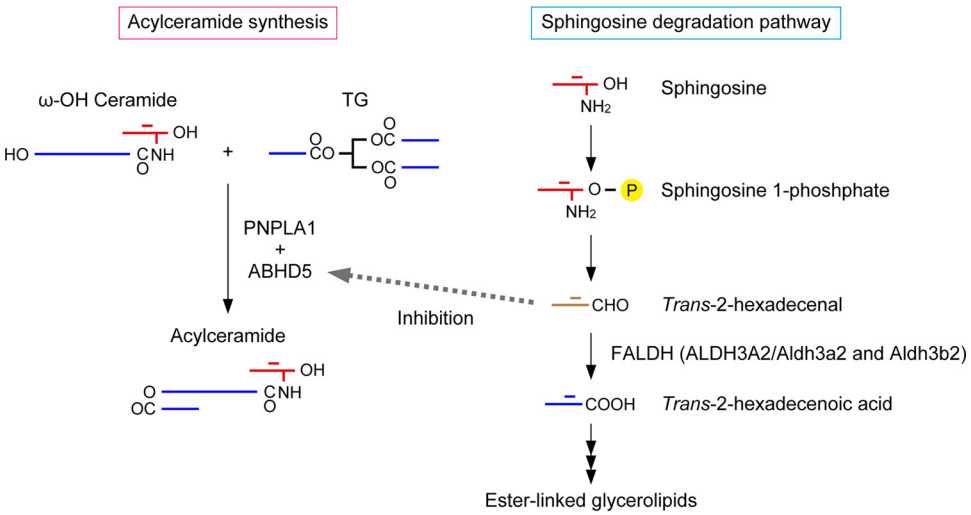

FIG 11 A model for reduced acylceramide production in SLS. Acylceramides are produced from ω-OH ceramide and TG via a transacylation reaction (left). The LCB sphingosine is converted to *trans*-2-hexadecenal in the degradation pathway and further metabolized to ester-linked glycerolipids under normal conditions (right). Under FALDH-deficient conditions, such as *ALDH3A2* mutation in humans (SLS) and *Aldh3a2 Aldh3b2* DKO in mice, the accumulated *trans*-2-hexadecenal attacks and inhibits ABHD5, resulting in reduced acylceramide production.

His residue conserved in the α/β hydrolase family. Therefore, ABHD5 meets the above-mentioned criteria for the target protein of the long-chain aldehydes that accumulate in DKO mice and SLS patients.

Fatty aldehydes, substrates of ALDH3A2, are produced via various metabolic pathways and reactions, including the LCB degradation pathway, oxidation of fatty alcohols, degradation of ether phospholipids, lipid peroxidation, and the metabolism of leukotriene B_4 (5, 19). Of these, to date, only the LCB degradation pathway has been shown to be impaired by reduced FALDH activity levels in keratinocytes (Fig. 9) (10). Some of the long-chain aldehydes derived from the LCBs that accumulate in FALDH-deficient cells may cause SLS by attacking nearby proteins before they are metabolized to nontoxic ether-linked glycerolipids. In the LCB degradation pathway, long-chain aldehydes are produced in the ER, since sphingosine 1-phosphate lyase, which produces long-chain aldehydes, is localized there (48). Ceramides are abundant in the epidermis (dozens of times more so than in other tissues) (49), suggesting that the quantities of long-chain aldehydes produced by ceramide and LCB degradation are also much higher than in other tissues. Sphingosine is the major LCB that constitutes ceramides, and in its degradation pathway it is converted to α,β-unsaturated aldehyde *trans*-2-hexadecenal (Fig. 11), which can undergo a Michael addition reaction. *In vitro* experiments have shown that of all the nucleophilic amino acids, His forms the most stable adduct with *trans*-2-hexadecenal (36). Based on these considerations, we speculate that of the fatty aldehydes, the long-chain aldehydes produced in the LCB degradation pathway, especially *trans*-2-hexadecenal, play an important role in SLS pathogenesis.

In the present study, we established a faithful mouse model of SLS and found that a reduction in acylceramide levels is involved in SLS skin pathology. We also proposed the following model for the molecular mechanism of acylceramide reduction: long-chain aldehydes produced via the LCB degradation pathway inhibit the final step of acylceramide production, perhaps by inhibiting the activity of ABHD5 (Fig. 11). We were unfortunately not able to detect the formation of adducts between ABHD5 and *trans*-2-hexadecenal due to technical issues. Future technological developments, especially those providing increased detection sensitivity for these adducts, are needed to prove this. Finally, our findings suggest the possibility of inhibiting the LCB degradation pathway in SLS patients as a potential therapeutic application.

TABLE 1 DNA oligonucleotides and primers used in this study

Oligonucleotide DNA or primer	Sequence
Aldh3b2 KO-1	5′-CACCGAGCCTGGGTCGCTTCTTGC-3′
Aldh3b2 KO-2	5′-TTTGGCAAGAAGCGACCCAGGCTC-3′
Aldh3b2-1	5′-CGGACTCGGCCTACTGAGTTTCGGA-3′
Aldh3b2-2	5′-CAGTCTGTGCATAGAGCAAGGG-3′
Aldh3a1-F	5′-CGGTGATGCCCATTGTGTGTGTTCG-3′
Aldh3a1-R	5′-TTCTTCATTCCGCAGAGACCTCACC-3′
Aldh3a2-F	5′-TTCTCGTAACAATAAGCTCATCAAACG-3′
Aldh3a2-R	5′-CAGCATCCCCAGCCTTCCTTTGTTG-3′
Aldh3b1-F	5′-GCTGTATGCCTTCTCCAAGAGAAGC-3′
Aldh3b1-R	5′-GCAGCTGCAGCACCTCTCCTCCATGG-3′
Aldh3b2-F	5′-TGAGTTCATCAACCGGCGGGAGAAGC-3′
Aldh3b2-R	5′-GTTGTTGGTTCCAGGGACCATAAGG-3′
Aldh3b3-F	5′-CTTTATGCCTATTCCAACAACGCAG-3′
Aldh3b3-R	5′-GGGTGCAGCTCTCAGAGCCGATAGC-3′
Gapdh-F	5′-GAACGGGAAGCTCACTGGCATGGCC-3′
Gapdh-R	5′-TGTCATACCAGGAAATGAGCTTGAC-3′
Cyp4f39-F	5′-AGCATCTACGGGACCCACCACAACC-3′
Cyp4f39-R	5′-TGAGGGTAGAGGCTCTACATTGAGC-3′
Fatp4-F	5′-AATGGCCTCAGCCATCTGTGAG-3′
Fatp4-R	5′-AGAGGGTCCAGGTGTTCTGTGC-3′
Cers3-F	5′-CTGGCTTCCTCCAACAATAAAGTGG-3′
Cers3-R	5′-TCAAGTTACACTTCTTTGCCAGTCC-3′
Pnpla1-F	5′-CCCCACAAGCCTCTGCTGGTGGAGG-3′
Pnpla1-R	5′-TGGCCACTCACTCCCTCGGGGTAGC-3′
Abhd5-F	5′-ATCACACCTTAAAGAAGCTGAAGAG-3′
Abhd5-R	5′-AATGGATTCCACAAACTGATTCTCC-3′
Krt1-F	5′-TGAGCTGAAGAACATGCAAGA-3′
Krt1-R	5′-CATGTAAGCTGAATCCACATCC-3′
Krt5-F	5′-CAGAGCTGAGGAACATGCAG-3′
Krt5-F	5′-CATTCTCAGCCGTGGTACG-3′
Lor-F	5′-GGTTGCAACGGAGACAACA-3′
Lor-R	5′-CATGAGAAAGTTAAGCCCATCG-3′
Ivl-F	5′-ACACACTGCCAGTGACTGTTCCAGC-3′
Ivl-R	5′-CTTCTCCAGATGCAGTTCCTGTTCC-3′
Hprt-F	5′-GCTGACCTGCTGGATTACATTAAAG-3′
Hprt-R	5′-CTTAACCATTTTGGGGCTGTACTGC-3′
hALDH3A2 KO-1	5′-TGTGGTCAAATCGCTGCTTCGTTTT-3′
hALDH3A2 KO-2	5′-GAAGCAGCGATTTGACCACACGGTG-3′
hALDH3A2 KO-3	5′-TGCGGTTGGCAAAATTGTCAGTTTT-3′
hALDH3A2 KO-4	5′-TGACAATTTTGCCAACCGCACGGTG-3′
hALDH3A2-1	5′-GGCAGTGCAAGAGTTTGTGTTTCTC-3′
hALDH3A2-2	5′-AGGTATGGGGTTCAAGTACAAAGAG-3′

MATERIALS AND METHODS

Mice. The *Aldh3a2* KO mice used were described previously (10). *Aldh3b2* KO mice were created using the CRISPR/Cas9 system as follows. The guide RNA targeted the 24 bases adjacent to the protospacer flanking motif (PAM) sequence present in exon 2 of *Aldh3b2*. The oligonucleotide pair (primers Aldh3b2 KO-1 and Aldh3b2 KO-2) (Table 1) containing the guide RNA sequence were annealed and then cloned into the BbsI site of the CRISPR/Cas9 vector pX330 (Addgene, Watertown, MA). The resulting plasmid was injected into fertilized eggs of C57BL/6J mice. Genomic DNA was prepared from the tails of the pups born and then subjected to PCR using the primers Aldh3b2-1 and Aldh3b2-2 (Table 1) to amplify exon 2 of *Aldh3b2*. Subsequent sequencing analysis revealed that one of the mice contained an 8-bp deletion in exon 2. This mouse was crossed with a C57BL/6J mouse to generate *Aldh3b2*$^{+/-}$ mice. The *Aldh3b2*$^{+/-}$ mice were twice back-crossed with C57BL/6J mice. *Aldh3b2*$^{-/-}$ mice were created by crossing male and female *Aldh3b2*$^{+/-}$ mice. The *Aldh3b2*$^{-/-}$ mice obtained were crossed with *Aldh3a2*$^{+/-}$ mice, producing *Aldh3a2*$^{+/-}$ *Aldh3b2*$^{+/-}$ mice. *Aldh3a2*$^{+/-}$ *Aldh3b2*$^{-/-}$ mice were then obtained by crossing male and female *Aldh3a2*$^{+/-}$ *Aldh3b2*$^{+/-}$ mice. These *Aldh3a2*$^{+/-}$ *Aldh3b2*$^{+/-}$ mice were maintained by back-crossing with *Aldh3b2*$^{-/-}$ mice. *Aldh3a2*$^{-/-}$ *Aldh3b2*$^{-/-}$ (*Aldh3a2 Aldh3b2* DKO) mice were generated by mating *Aldh3a2*$^{+/-}$ *Aldh3b2*$^{-/-}$ mice with each other. Littermate *Aldh3a2*$^{+/+}$ *Aldh3b2*$^{-/-}$ (*Aldh3b2* KO) and DKO mice were used in the experiments. C57BL/6J mice born on the same day were used as WT controls for some experiments. Genotyping of the *Aldh3a2* gene was conducted as described previously (10).

Genotyping of the *Aldh3b2* gene was performed by PCR using genomic DNA prepared from mouse tails and the primers Aldh3b2-1 and Aldh3b2-2 (Table 1). The amplified DNA fragments of *Aldh3b2* were digested using the restriction enzyme MwoI, whose restriction enzyme recognition site is lost in *Aldh3b2* KO mice, and separated and identified using agarose gel electrophoresis.

Mice were housed under specific-pathogen-free conditions at a room temperature of 23°C ± 1°C, humidity of 50% ± 5%, and a light-dark cycle of 12 h:12 h, with food and water available *ad libitum*. All animal experiments were approved by the institutional animal care and use committee of Hokkaido University (permit 17-0017).

Cells and transfection. Human immortalized keratinocytes (NHEK/SVTERT3-5) were purchased from Evercyte (Vienna, Austria). Cells were cultured in CnT-Prime epithelial culture medium (CELLnTEC, Bern, Switzerland) in dishes coated with 0.3% collagen (Nitta Gelatin, Osaka, Japan) at 37°C in the presence of 5% CO_2. Transfection was performed using ViaFect transfection reagent (Promega, Madison, WI), according to the manufacturer's manual. For differentiation, cells were grown in 12-well dishes to almost 100% confluence, and then the medium was replaced with CnT-Prime epithelial 3D barrier medium (CnT-3D; CELLnTEC) supplemented with linoleic acid (10 μM). The cells were cultured for 14 days, with the medium refreshed every 3 days.

Generation of *ALDH3A2* KO cells. To generate *ALDH3A2* KO human immortalized keratinocytes, we used an all-in-one CRISPR/Cas9 vector, pYU417 (50), which consisted of a Cas9 D10A mutant nuclease (Cas9 nickase) gene, a guide RNA cloning cassette, *EGFP*, and a puromycin *N*-acetyltransferase gene. Two targets, each of which consisted of 20 bases adjacent to the PAM sequence in exon 4 of *ALDH3A2* (Fig. 10A), were selected for the guide RNAs. Each of a pair of oligonucleotides (hALDH3A2 KO-1/2 or hALDH3A2 KO-3/4) (Table 1) corresponding to the respective guide RNA sequence was annealed and cloned into the BaeI site of pYU417. Human immortalized keratinocytes were transfected simultaneously with both of the resulting plasmids. At 24 h after transfection, the cells were cultured for 48 h in KGM-2 keratinocyte growth medium (Lonza, Basel, Switzerland) containing 2 μg/ml puromycin to select the cells containing the plasmids. The medium was then replaced with puromycin-free CnT-Prime epithelial culture medium, and the cells were cultured for another 2 days. Cells were detached from the dishes by treatment with 0.05% trypsin-EDTA (Thermo Fisher Scientific, Waltham, MA), diluted, seeded into 10-cm dishes, and cultured for 7 days. Several clones were selected and cultured in 12-well plates. Genomic DNA was prepared from the cells, and DNA fragments containing the target sequence of *ALDH3A2* were amplified via PCR using the primers hALDH3A2-1 and hALDH3A2-2 (Table 1), followed by DNA sequencing. Two clones with mutations in *ALDH3A2* (KO clones 1 and 2) were used for the subsequent experiments. As control cells, two clones (control clones 1 and 2) were generated using the same method but with an empty pYU417 vector.

Skin permeability barrier assays. TEWL was measured from the backs of P0 mice using an AS-VT100RS evaporimeter (Asch Japan, Tokyo, Japan). Toluidine blue staining was performed as previously described (22), except for the staining time. Briefly, mice were soaked in methanol for 5 min, washed with phosphate-buffered saline (PBS), incubated with 0.1% toluidine blue solution at 4°C for 40 h, washed with PBS, and photographed.

FALDH assay. FALDH activity was measured as described previously (10).

Histological analyses. The skin of the P0 mice was prepared from their backs and analyzed via hematoxylin and eosin staining (10) or transmission electron microscopy (33), as described previously. Scanning electron microscopy was performed as follows. Skin from the heads of the P0 mice was fixed with 2% paraformaldehyde and 2% glutaraldehyde in 0.1 M cacodylate buffer (pH 7.4) at 4°C overnight and further fixed with 0.1% tannic acid in 0.1 M cacodylate buffer (pH 7.4) at 4°C overnight. After washing with 0.1 M cacodylate buffer (pH 7.4) four times for 30 min each, samples were postfixed with 2% osmium tetroxide in 0.1 M cacodylate buffer (pH 7.4) at 4°C overnight. The samples were dehydrated in graded ethanol solutions as follows: 50% and 70% ethanol, at 4°C for 1 h each; 90% ethanol at room temperature for 1 h; 100% ethanol four times at room temperature for 1 h each; and 100% ethanol at room temperature overnight. To freeze-dry the samples, we treated them with a 1:1 mixture of ethanol and *tert*-butyl alcohol at room temperature for 2 h and then with 100% *tert*-butyl alcohol three times at room temperature for 1 h each, froze them at 4°C, and vacuum dried. The samples were coated with a thin layer (50 nm) of osmium using an osmium plasma coater (NL-OPC80A; Nippon Laser and Electronics Laboratory, Nagoya, Japan) and observed using a scanning electron microscope (JSM-6340F; JEOL, Tokyo, Japan) at an acceleration voltage of 5.0 kV.

Lipid analyses. Lipids were extracted from the epidermis as described previously (23) and subjected to LC-MS/MS analyses and TLC separation. For TLC separation suitable for ceramides, silica gel 60 TLC plates (Merck Millipore, Darmstadt, Germany) and a previously described solvent system (24) were used. For TLC separation suitable for the less polar lipids, silica gel 60 high-performance TLC plates (Merck Millipore) and the resolving buffer (hexane-diethyl ether-acetic acid, 65:35:1 [vol/vol/vol]) were used, and lipids were developed to the top of the TLC plates, dried, and developed to the top again. They were stained with copper phosphate reagent as described previously (23).

Lipid analyses via LC-MS/MS were performed using a triple-quadrupole mass spectrometer (Xevo TQ-S; Waters, Milford, MA) in multiple-reaction-monitoring mode. Ionization was performed using electrospray ionization. The conditions of LC separation and electrospray ionization were as described previously (51). Prior to LC-MS/MS, FAs and OAHFAs were derivatized to *N*-(4-aminomethylphenyl)pyridinium (AMPP) amides using the AMP+ mass spectrometry kit (Cayman Chemical, Ann Arbor, MI) according to the manufacturer's manual. The *m/z* values of the precursor ion (Q1) and product ion (Q3) and the collision energies used were as previously reported for the ceramides, acylceramides, ω-OH ceramides, protein-bound ceramides, TGs, and FAs (23) and as reported elsewhere for the OAHFAs (52). For

quantitation of the ceramides, ω-OH ceramides, protein-bound ceramides, acylceramides, and TGs, *N*-palmitoyl(d_9)-D-*erythro*-sphingosine ($C_{16:0}$ ceramide; Avanti Polar Lipids, Alabaster, AL), *N*-ω-hydroxytriacontanoyl-D-*erythro*-sphingosine ($C_{30:0}$ ω-OH ceramide; Cayman Chemical), *N*-(30-linoleoyloxy-triacontanoyl)-sphingosine ($C_{30:0}$ acylceramide; Cayman Chemical), and 1,3-dipentadecanoyl-2-oleoyl(d_7)-glycerol (Avanti Polar Lipids) were used as external standards. To quantitate the FAs, palmitic acid-d_{31} (Cayman Chemical) was used as an internal standard. Absolute quantification was not performed for OAHFAs, since no standard is commercially available.

Lipid analyses for the mouse SC samples were performed essentially as described previously (51), except that the quantities of tape, internal standards, and solvent used were double those in that report. The lipid analyses for the differentiated human keratinocytes were as follows. Cells grown in 12-well dishes were washed twice with 500 μl of PBS, suspended in 300 μl of PBS, detached from the dishes using a scraper, and transferred to microcentrifuge tubes. After centrifugation (400 $\times$ *g*, room temperature, 3 min), the cells were suspended in 150 μl of water and lysed by sonication. Samples were divided into 50 μl and 100 μl; the former was used for protein quantification and the latter for lipid extraction. Lipids were extracted via the successive addition and mixing of 375 μl of chloroform-methanol (1:2 [vol/vol]), 125 μl of chloroform, and 125 μl of water. Phases were separated by centrifugation (20,000 $\times$ *g*, room temperature, 3 min), and the lower phase (organic phase) was collected and dried. The dried lipids were dissolved in chloroform-methanol (1:2 [vol/vol]) to a concentration of 0.3 μg protein/μl. LC-MS/MS analyses and the internal standards used were as described previously (51).

Quantitative real-time RT-PCR. P0 mouse skin was suspended in 600 μl PBS and incubated at 55°C for 5 min to separate the epidermis and dermis. Total epidermal RNA was prepared using a NucleoSpin RNA II kit (Macherey-Nagel, Dueren, Germany) according to the manufacturer's protocol. Quantitative real-time RT-PCR was performed using a One-Step SYBR PrimeScript RT-PCR kit II (TaKaRa Bio, Shiga, Japan) and forward (F) and reverse (R) primer pairs (Table 1) as described previously (24).

[^{3}H]DHS labeling assay. Primary keratinocytes were prepared from the mice, cultured, and differentiated as described previously (10). The [^{3}H]DHS labeling assay was conducted as described previously (31).

ACKNOWLEDGMENTS

We thank Tatsuro Naganuma and Chifumi Yagi for technical support and discussions.

This work was supported by the Advanced Research and Development Programs for Medical Innovation (AMED-CREST) (grant JP20gm0910002h0006 to A.K.) from the Japan Agency for Medical Research and Development (AMED) and by KAKENHI (grant JP18H03976 to A.K.) from the Japan Society for the Promotion of Science.

REFERENCES

1. Marchitti SA, Brocker C, Stagos D, Vasiliou V. 2008. Non-P450 aldehyde oxidizing enzymes: the aldehyde dehydrogenase superfamily. Expert Opin Drug Metab Toxicol 4:697–720. https://doi.org/10.1517/17425255.4.6.697.
2. Jackson B, Brocker C, Thompson DC, Black W, Vasiliou K, Nebert DW, Vasiliou V. 2011. Update on the aldehyde dehydrogenase gene (ALDH) superfamily. Hum Genomics 5:283–303. https://doi.org/10.1186/1479-7364-5-4-283.
3. Vasiliou V, Pappa A. 2000. Polymorphisms of human aldehyde dehydrogenases: consequences for drug metabolism and disease. Pharmacology 61:192–198. https://doi.org/10.1159/000028400.
4. Sjögren T, Larsson T. 1957. Oligophrenia in combination with congenital ichthyosis and spastic disorders; a clinical and genetic study. Acta Psychiatr Neurol Scand Suppl 113:1–112.
5. Rizzo WB. 2014. Fatty aldehyde and fatty alcohol metabolism: review and importance for epidermal structure and function. Biochim Biophys Acta 1841:377–389. https://doi.org/10.1016/j.bbalip.2013.09.001.
6. Rizzo WB. 2007. Sjögren-Larsson syndrome: molecular genetics and biochemical pathogenesis of fatty aldehyde dehydrogenase deficiency. Mol Genet Metab 90:1–9. https://doi.org/10.1016/j.ymgme.2006.08.006.
7. Cho KH, Shim SH, Kim M. 2018. Clinical, biochemical, and genetic aspects of Sjögren-Larsson syndrome. Clin Genet 93:721–730. https://doi.org/10.1111/cge.13058.
8. Rizzo WB, Carney G. 2005. Sjögren-Larsson syndrome: diversity of mutations and polymorphisms in the fatty aldehyde dehydrogenase gene (*ALDH3A2*). Hum Mutat 26:1–10. https://doi.org/10.1002/humu.20181.
9. Kanetake T, Sassa T, Nojiri K, Sawai M, Hattori S, Miyakawa T, Kitamura T, Kihara A. 2019. Neural symptoms in a gene knockout mouse model of Sjögren-Larsson syndrome are associated with a decrease in 2-hydroxygalactosylceramide. FASEB J 33:928–941. https://doi.org/10.1096/fj.201800291R.
10. Naganuma T, Takagi S, Kanetake T, Kitamura T, Hattori S, Miyakawa T, Sassa T, Kihara A. 2016. Disruption of the Sjögren-Larsson syndrome gene *Aldh3a2* in mice increases keratinocyte growth and retards skin barrier recovery. J Biol Chem 291:11676–11688. https://doi.org/10.1074/jbc.M116.714030.
11. Kitamura T, Takagi S, Naganuma T, Kihara A. 2015. Mouse aldehyde dehydrogenase ALDH3B2 is localized to lipid droplets via two C-terminal tryptophan residues and lipid modification. Biochem J 465:79–87. https://doi.org/10.1042/BJ20140624.
12. Kelson TL, Secor McVoy JR, Rizzo WB. 1997. Human liver fatty aldehyde dehydrogenase: microsomal localization, purification, and biochemical characterization. Biochim Biophys Acta 1335:99–110. https://doi.org/10.1016/s0304-4165(96)00126-2.
13. Kitamura T, Naganuma T, Abe K, Nakahara K, Ohno Y, Kihara A. 2013. Substrate specificity, plasma membrane localization, and lipid modification of the aldehyde dehydrogenase ALDH3B1. Biochim Biophys Acta 1831:1395–1401. https://doi.org/10.1016/j.bbalip.2013.05.007.
14. Traupe H, Fischer J, Oji V. 2014. Nonsyndromic types of ichthyoses—an update. J Dtsch Dermatol Ges 12:109–121. https://doi.org/10.1111/ddg.12229.
15. Goleva E, Berdyshev E, Leung DY. 2019. Epithelial barrier repair and prevention of allergy. J Clin Invest 129:1463–1474. https://doi.org/10.1172/JCI124608.
16. Bouwstra JA, Ponec M. 2006. The skin barrier in healthy and diseased state. Biochim Biophys Acta 1758:2080–2095. https://doi.org/10.1016/j.bbamem.2006.06.021.
17. Hirabayashi T, Murakami M, Kihara A. 2019. The role of PNPLA1 in ω-*O*-acylceramide synthesis and skin barrier function. Biochim Biophys Acta Mol Cell Biol Lipids 1864:869–879. https://doi.org/10.1016/j.bbalip.2018.09.010.
18. Feingold KR, Elias PM. 2014. Role of lipids in the formation and maintenance of the cutaneous permeability barrier. Biochim Biophys Acta 1841:280–294. https://doi.org/10.1016/j.bbalip.2013.11.007.

19. Kihara A. 2016. Synthesis and degradation pathways, functions, and pathology of ceramides and epidermal acylceramides. Prog Lipid Res 63:50–69. https://doi.org/10.1016/j.plipres.2016.04.001.
20. Takeichi T, Akiyama M. 2016. Inherited ichthyosis: non-syndromic forms. J Dermatol 43:242–251. https://doi.org/10.1111/1346-8138.13243.
21. Breiden B, Sandhoff K. 2014. The role of sphingolipid metabolism in cutaneous permeability barrier formation. Biochim Biophys Acta 1841:441–452. https://doi.org/10.1016/j.bbalip.2013.08.010.
22. Sassa T, Ohno Y, Suzuki S, Nomura T, Nishioka C, Kashiwagi T, Hirayama T, Akiyama M, Taguchi R, Shimizu H, Itohara S, Kihara A. 2013. Impaired epidermal permeability barrier in mice lacking *Elovl1*, the gene responsible for very-long-chain fatty acid production. Mol Cell Biol 33:2787–2796. https://doi.org/10.1128/MCB.00192-13.
23. Yamamoto H, Hattori M, Chamulitrat W, Ohno Y, Kihara A. 2020. Skin permeability barrier formation by the ichthyosis-causative gene *FATP4* through formation of the barrier lipid ω-*O*-acylceramide. Proc Natl Acad Sci U S A 117:2914–2922. https://doi.org/10.1073/pnas.1917525117.
24. Miyamoto M, Itoh N, Sawai M, Sassa T, Kihara A. 2020. Severe skin permeability barrier dysfunction in knockout mice deficient in a fatty acid ω-hydroxylase crucial to acylceramide production. J Invest Dermatol 140:319–326. https://doi.org/10.1016/j.jid.2019.07.689.
25. Rizzo WB. 2011. The role of fatty aldehyde dehydrogenase in epidermal structure and function. Dermatoendocrinology 3:91–99. https://doi.org/10.4161/derm.3.2.14619.
26. Ohno Y, Kamiyama N, Nakamichi S, Kihara A. 2017. PNPLA1 is a transacylase essential for the generation of the skin barrier lipid ω-*O*-acylceramide. Nat Commun 8:14610. https://doi.org/10.1038/ncomms14610.
27. Muñoz-Garcia A, Thomas CP, Keeney DS, Zheng Y, Brash AR. 2014. The importance of the lipoxygenase-hepoxilin pathway in the mammalian epidermal barrier. Biochim Biophys Acta 1841:401–408. https://doi.org/10.1016/j.bbalip.2013.08.020.
28. Takeichi T, Hirabayashi T, Miyasaka Y, Kawamoto A, Okuno Y, Taguchi S, Tanahashi K, Murase C, Takama H, Tanaka K, Boeglin WE, Calcutt MW, Watanabe D, Kono M, Muro Y, Ishikawa J, Ohno T, Brash AR, Akiyama M. 2020. SDR9C7 catalyzes critical dehydrogenation of acylceramides for skin barrier formation. J Clin Invest 130:890–903. https://doi.org/10.1172/JCI130675.
29. Elias PM, Gruber R, Crumrine D, Menon G, Williams ML, Wakefield JS, Holleran WM, Uchida Y. 2014. Formation and functions of the corneocyte lipid envelope (CLE). Biochim Biophys Acta 1841:314–318. https://doi.org/10.1016/j.bbalip.2013.09.011.
30. Ohno Y, Nara A, Nakamichi S, Kihara A. 2018. Molecular mechanism of the ichthyosis pathology of Chanarin-Dorfman syndrome: stimulation of PNPLA1-catalyzed ω-*O*-acylceramide production by ABHD5. J Dermatol Sci 92:245–253. https://doi.org/10.1016/j.jdermsci.2018.11.005.
31. Nakahara K, Ohkuni A, Kitamura T, Abe K, Naganuma T, Ohno Y, Zoeller RA, Kihara A. 2012. The Sjögren-Larsson syndrome gene encodes a hexadecenal dehydrogenase of the sphingosine 1-phosphate degradation pathway. Mol Cell 46:461–471. https://doi.org/10.1016/j.molcel.2012.04.033.
32. Nakajima K, Sano S, Uchida Y, Akiyama M, Morita Y, Shimizu H. 2011. Altered lipid profiles in the stratum corneum of Sjögren-Larsson syndrome. J Dermatol Sci 63:64–66. https://doi.org/10.1016/j.jdermsci.2011.03.009.
33. Honda Y, Kitamura T, Naganuma T, Abe T, Ohno Y, Sassa T, Kihara A. 2018. Decreased skin barrier lipid acylceramide and differentiation-dependent gene expression in ichthyosis gene *Nipal4*-knockout mice. J Invest Dermatol 138:741–749. https://doi.org/10.1016/j.jid.2017.11.008.
34. Jennemann R, Rabionet M, Gorgas K, Epstein S, Dalpke A, Rothermel U, Bayerle A, van der Hoeven F, Imgrund S, Kirsch J, Nickel W, Willecke K, Riezman H, Grone HJ, Sandhoff R. 2012. Loss of ceramide synthase 3 causes lethal skin barrier disruption. Hum Mol Genet 21:586–608. https://doi.org/10.1093/hmg/ddr494.
35. Catalá A. 2009. Lipid peroxidation of membrane phospholipids generates hydroxy-alkenals and oxidized phospholipids active in physiological and/or pathological conditions. Chem Phys Lipids 157:1–11. https://doi.org/10.1016/j.chemphyslip.2008.09.004.
36. Schumacher F, Neuber C, Finke H, Nieschalke K, Baesler J, Gulbins E, Kleuser B. 2017. The sphingosine 1-phosphate breakdown product, (2*E*)-hexadecenal, forms protein adducts and glutathione conjugates *in vitro*. J Lipid Res 58:1648–1660. https://doi.org/10.1194/jlr.M076562.
37. Ashibe B, Hirai T, Higashi K, Sekimizu K, Motojima K. 2007. Dual subcellular localization in the endoplasmic reticulum and peroxisomes and a vital role in protecting against oxidative stress of fatty aldehyde dehydrogenase are achieved by alternative splicing. J Biol Chem 282:20763–20773. https://doi.org/10.1074/jbc.M611853200.
38. Eckhardt M, Yaghootfam A, Fewou SN, Zöller I, Gieselmann V. 2005. A mammalian fatty acid hydroxylase responsible for the formation of α-hydroxylated galactosylceramide in myelin. Biochem J 388:245–254. https://doi.org/10.1042/BJ20041451.
39. Zhu G, Koszelak-Rosenblum M, Connelly SM, Dumont ME, Malkowski MG. 2015. The crystal structure of an integral membrane fatty acid α-hydroxylase. J Biol Chem 290:29820–29833. https://doi.org/10.1074/jbc.M115.680124.
40. Hama H. 2010. Fatty acid 2-hydroxylation in mammalian sphingolipid biology. Biochim Biophys Acta 1801:405–414. https://doi.org/10.1016/j.bbalip.2009.12.004.
41. Zöller I, Meixner M, Hartmann D, Büssow H, Meyer R, Gieselmann V, Eckhardt M. 2008. Absence of 2-hydroxylated sphingolipids is compatible with normal neural development but causes late-onset axon and myelin sheath degeneration. J Neurosci 28:9741–9754. https://doi.org/10.1523/JNEUROSCI.0458-08.2008.
42. Potter KA, Kern MJ, Fullbright G, Bielawski J, Scherer SS, Yum SW, Li JJ, Cheng H, Han X, Venkata JK, Khan PA, Rohrer B, Hama H. 2011. Central nervous system dysfunction in a mouse model of FA2H deficiency. Glia 59:1009–1021. https://doi.org/10.1002/glia.21172.
43. Lass A, Zimmermann R, Haemmerle G, Riederer M, Schoiswohl G, Schweiger M, Kienesberger P, Strauss JG, Gorkiewicz G, Zechner R. 2006. Adipose triglyceride lipase-mediated lipolysis of cellular fat stores is activated by CGI-58 and defective in Chanarin-Dorfman syndrome. Cell Metab 3:309–319. https://doi.org/10.1016/j.cmet.2006.03.005.
44. Yang A, Mottillo EP, Mladenovic-Lucas L, Zhou L, Granneman JG. 2019. Dynamic interactions of ABHD5 with PNPLA3 regulate triacylglycerol metabolism in brown adipocytes. Nat Metab 1:560–569. https://doi.org/10.1038/s42255-019-0066-3.
45. Lord CC, Thomas G, Brown JM. 2013. Mammalian alpha beta hydrolase domain (ABHD) proteins: lipid metabolizing enzymes at the interface of cell signaling and energy metabolism. Biochim Biophys Acta 1831:792–802. https://doi.org/10.1016/j.bbalip.2013.01.002.
46. Brown AL, Mark Brown J. 2017. Critical roles for α/β hydrolase domain 5 (ABHD5)/comparative gene identification-58 (CGI-58) at the lipid droplet interface and beyond. Biochim Biophys Acta Mol Cell Biol Lipids 1862:1233–1241. https://doi.org/10.1016/j.bbalip.2017.07.016.
47. Hirabayashi T, Anjo T, Kaneko A, Senoo Y, Shibata A, Takama H, Yokoyama K, Nishito Y, Ono T, Taya C, Muramatsu K, Fukami K, Munoz-Garcia A, Brash AR, Ikeda K, Arita M, Akiyama M, Murakami M. 2017. PNPLA1 has a crucial role in skin barrier function by directing acylceramide biosynthesis. Nat Commun 8:14609. https://doi.org/10.1038/ncomms14609.
48. Ikeda M, Kihara A, Igarashi Y. 2004. Sphingosine-1-phosphate lyase SPL is an endoplasmic reticulum-resident, integral membrane protein with the pyridoxal 5′-phosphate binding domain exposed to the cytosol. Biochem Biophys Res Commun 325:338–343. https://doi.org/10.1016/j.bbrc.2004.10.036.
49. Edagawa M, Sawai M, Ohno Y, Kihara A. 2018. Widespread tissue distribution and synthetic pathway of polyunsaturated C24:2 sphingolipids in mammals. Biochim Biophys Acta Mol Cell Biol Lipids 1863:1441–1448. https://doi.org/10.1016/j.bbalip.2018.09.002.
50. Sawai M, Uchida Y, Ohno Y, Miyamoto M, Nishioka C, Itohara S, Sassa T, Kihara A. 2017. The 3-hydroxyacyl-CoA dehydratases HACD1 and HACD2 exhibit functional redundancy and are active in a wide range of fatty acid elongation pathways. J Biol Chem 292:15538–15551. https://doi.org/10.1074/jbc.M117.803171.
51. Kawana M, Miyamoto M, Ohno Y, Kihara A. 2020. Comparative profiling and comprehensive quantification of stratum corneum ceramides in humans and mice by LC/MS/MS. J Lipid Res 61:884–895. https://doi.org/10.1194/jlr.RA120000671.
52. Miyamoto M, Sassa T, Sawai M, Kihara A. 2020. Lipid polarity gradient formed by ω-hydroxy lipids in tear film prevents dry eye disease. Elife 9:e53582. https://doi.org/10.7554/eLife.53582.